Can. J. Remote Sensing, Vol. 36, Suppl. 2, pp. S211–S223, 2010

Research note / Note de recherche

Quantifying errors in discontinuous permafrost plateau change from optical data, Northwest Territories, Canada: 1947–2008

L. Chasmer, C. Hopkinson, and W. Quinton

Abstract. The discontinuous permafrost zone has been subject to increased air temperatures over recent decades. Permafrost thaw can cause changes to topography, hydrology, vegetation, and trace gas fluxes, and thus it is important to monitor changes in permafrost area through time. Optical imagery can be used to generate time-series databases of near-surface spectra that may be related to permafrost area. This provides a spatial perspective on area permafrost change that is not easily obtained from field data alone. This study examines the cumulative maximum and minimum errors of aerial and satellite imagery used for change detection within the Scotty Creek watershed, Fort Simpson, NWT, Canada. The results illustrate that, unless unchanging linear features are found throughout every image used (e.g., to be used as multitemporal tie points) and radiometric normalization can be applied (problematic for film images), direct image to image comparisons (e.g., subtraction) are not appropriate. Further, measureable cumulative errors are often produced by misclassification of edges, resolution limitations, and increased landscape fragmentation. At Scotty Creek, increased fragmentation of permafrost plateaus occurred from 1947 to 2008. Cumulative maximum and minimum errors result in an approximate 8%–26% error in permafrost area when compared with the total area of the site. Rates of permafrost area reduction within the study area were approximately 0.5% every year, determined from linear correlation ($r^2 = 0.91$, $n = 5$). Therefore, based on the maximum cumulative error (a worst-case scenario), approximately 21–32 years (for resolutions of 0.18–1.10 m) is required between images to approximate change within this particular site. Increased (decreased) rates of change at other sites will decrease (increase) the timing required to identify change between images beyond error bounds.

Résumé. La zone de pergélisol discontinu a été soumise à un accroissement des températures de l'air au cours des dernières décennies. Le dégel du pergélisol peut entraîner des changements dans la topographie, l'hydrologie, la végétation et les flux de gaz à l'état de traces, d'où l'importance de faire le suivi temporel de la superficie du pergélisol. Les images optiques peuvent être utilisées pour générer des bases de données de séries chronologiques des spectres près de la surface qui peuvent être reliés à la superficie du pergélisol. Ceci donne une perspective spatiale sur l'état du changement de la superficie du pergélisol qui n'est pas facilement obtenue à l'aide des seules données de terrain. Dans cette étude, on examine les erreurs cumulatives maximales et minimales des images aéroportées et satellitaires utilisées pour la détection du changement dans le bassin hydrographique de Scotty Creek, Fort Simpson, TNW, Canada. Les résultats démontrent qu'à moins qu'il y ait des caractéristiques linéaires invariables sur l'ensemble des images utilisées (p. ex. pour être utilisées comme points de raccordement multitemporels) et que la normalisation radiométrique puisse être appliquée (ce qui est problématique dans le cas des images sur film), les comparaisons directes image à image (p. ex. soustraction) ne sont pas appropriées. De plus, des erreurs cumulatives mesurables sont souvent produites par la classification erronée des contours, les limites de la résolution et la fragmentation accrue du paysage. À Scotty Creek, la fragmentation accrue des plateaux de pergélisol s'est produite de 1947 à 2008. Des erreurs cumulatives maximales et minimales résultent en une erreur approximative de 8 % à 26 % dans la superficie du pergélisol comparativement à la surface totale du site. Les taux de réduction de la superficie du pergélisol à l'intérieur de la zone d'étude étaient approximativement de 0,5 % à chaque année, établis à partir d'une corrélation linéaire ($r^2 = 0{,}91$, $n = 5$). Ainsi, basé sur l'erreur cumulative maximale (un scénario extrême), une période variant de 21 à 32 années approximativement (pour les résolutions de 0,18 m à 1,10 m) est requise entre les images pour approximer le changement à l'intérieur de ce site particulier. Des taux croissants (décroissants) de changement pour d'autres sites réduiront (augmenteront) l'échelle temporelle requise permettant d'identifier le changement entre les images au-delà des bornes d'erreur.
[Traduit par la Rédaction]

Received 20 September 2009. Accepted 30 March 2010. Published on the Web at http://pubservices.nrc-cnrc.ca/cjrs on 21 January 2011.

L. Chasmer[1] and W. Quinton. Cold Regions Research Centre, Wilfrid Laurier University, Waterloo, ON N2L 3C5, Canada.

C. Hopkinson. Applied Geomatics Research Group 2, NSCC Annapolis Valley Campus, 50 Elliott Road, RR1 Lawrencetown, NS B0S 1M0, Canada.

[1]Corresponding author (e-mail: lechasme@yahoo.ca).

Introduction

Accurate quantification of vegetation and permafrost plateau area change during periods of climatic warming is an important issue for management of northern infrastructure (Hinzman et al., 2005) and natural resources assessment (Quinton and Hayashi, 2007; Quinton et al., 2009). Permafrost is especially sensitive to climatic warming because small increases in ground heating result in large changes to the surface hydrology (Rouse, 2000; Hayashi et al., 2004; Quinton et al., 2005). Typically, permafrost thaw is quantified by measuring the depth to the active (i.e., seasonally thawed) layer below the soil surface at varying temporal resolutions ranging from daily to interannually (e.g., Leverington and Duguay, 1997; Quinton et al., 2009; Chasmer et al., 2010). However, such measurements can be prohibitively expensive and difficult to obtain within northern upland–wetland ecosystems. To reduce the costs associated with in situ measurements of permafrost thaw, remote sensing (RS) of vegetation cover may be employed as a proxy for permafrost plateau area change. Previous studies have shown that vegetation cover at the individual tree to landscape scale is strongly correlated with the spatial distribution of permafrost plateaus within the subarctic, including approximately 53 000 km^2 of the lower Liard River valley (e.g., McMichael et al., 1997; Tutubalina and Rees, 2001; Wright et al., 2009; Chasmer et al., 2010). Trees tend to grow on plateaus and eventually perish at plateau edges due to waterlogging (from meltwater runoff).

High-resolution aerial photography, digital imagery, airborne light detection and ranging (lidar), and satellite imagery can be used to assess changes in vegetation cover and permafrost thaw over long time periods (Tutubalina and Rees, 2001; Beilman and Robinson, 2003). Passive RS of visible (VIS) and near-infrared (NIR) wavelengths from aerial and (or) satellite imagery may be used to infer variations in land cover type and properties across imaged regions. Stereo photographs, an important product of optical aerial photography, are often used to estimate variations in ground surface elevation. Ground surface elevation is also measured directly using airborne lidar. Lidar is an active technology that, unlike passive RS, measures the location of objects at or near the Earth's surface by rapidly emitting pulses of laser light at a spectral wavelength of 1064 nm (in this case). Objects scatter light as reflections or "returns" that are detectable (and within the proprietary waveform specifications) by the sensor optics. Returns are then converted into multiple distances based on timing of laser emission (pulse) to reception (return). Range information is then combined with positional data generated by an onboard position orientation system, including an inertial measurement unit and kinematic global positioning system (GPS) (plus local ground base station), to determine the x, y, and z coordinates and the intensity of the return (Wehr and Lohr, 1999).

Subdecametre-resolution (<10 m) RS images have many advantages for quantifying permafrost area change: (*i*) for many parts of Canada, the temporal coverage of available aerial photography extends back to the first half of the 20th century, providing a relatively long historical record for analysis (Mars and Houseknecht, 2007; Lantuit and Pollard, 2008); (*ii*) unlike field measurements made along individual transects, RS data provide continuous coverage (e.g., McMichael et al., 1997; Boike and Yoshikawa, 2003); (*iii*) archived aerial photography and satellite imagery typically cost much less than in situ measurements (Zhang et al., 2004); and (*iv*) if airborne lidar data are used, lidar provides a direct measurement of ground elevation, which is important for aerial triangulation and orthorectification of historical imagery. Lidar is also particularly useful for identifying areas of raised elevation (0.5–2.0 m, typical of permafrost plateaus) surrounded by bogs and fens (Robinson and Moore, 2000).

There are numerous disadvantages to the use of high-resolution RS data (<10 m) for quantifying permafrost area change: (*i*) several years may separate acquisition times of RS data, and therefore detailed daily, seasonal, and annual processes cannot be assessed (Zhang et al., 2004); (*ii*) differences in the time of photograph–image acquisition (plant phenology, solar angles, soil moisture), the imaging scale used, and the orthorectification process lead to compounded and often unquantified errors within change detection analysis (e.g., Riordan et al., 2006); and (*iii*) lidar data acquisitions are expensive within remote areas (due to air travel and equipment transport), although costs may be similar to those of in situ fieldwork. Despite some disadvantages as to the application of high-resolution RS data for monitoring landscape evolution, the availability of long historical records is unique to aerial photography, thereby justifying their use as a basis for landscape monitoring.

This study attempts to quantify errors in historical aerial photography, satellite imagery, and high-resolution digital image interpretation of permafrost plateau areas from 1947 to 2008. Based on cumulative errors and the rate of plateau conversion to fen–bog, suggestions are made as to the temporal interval required to observe discernable change in plateau area, at this site, using RS image analysis techniques.

Study area

The Scotty Creek watershed study area (61.44°N, 121.25°W) is located within the lower Liard River valley of the Northwest Territories, Canada (**Figure 1**). The site is within the discontinuous permafrost zone and is classified as high boreal wetland by the National Wetlands Working Group (1988). The watershed is comprised of upland, treed permafrost plateaus, elongated fens, and circular–rectangular bogs (Wright et al., 2009) and extends over an area of approximately 152 km^2. In this study, a subset area of 900 m × 1150 m was examined (due to the area of the lidar survey and the existence of definable linear features required for orthorectification of historical imagery).

Permafrost plateaus and permafrost-free fens and bogs are geometrically and spectrally distinct, within the VIS and

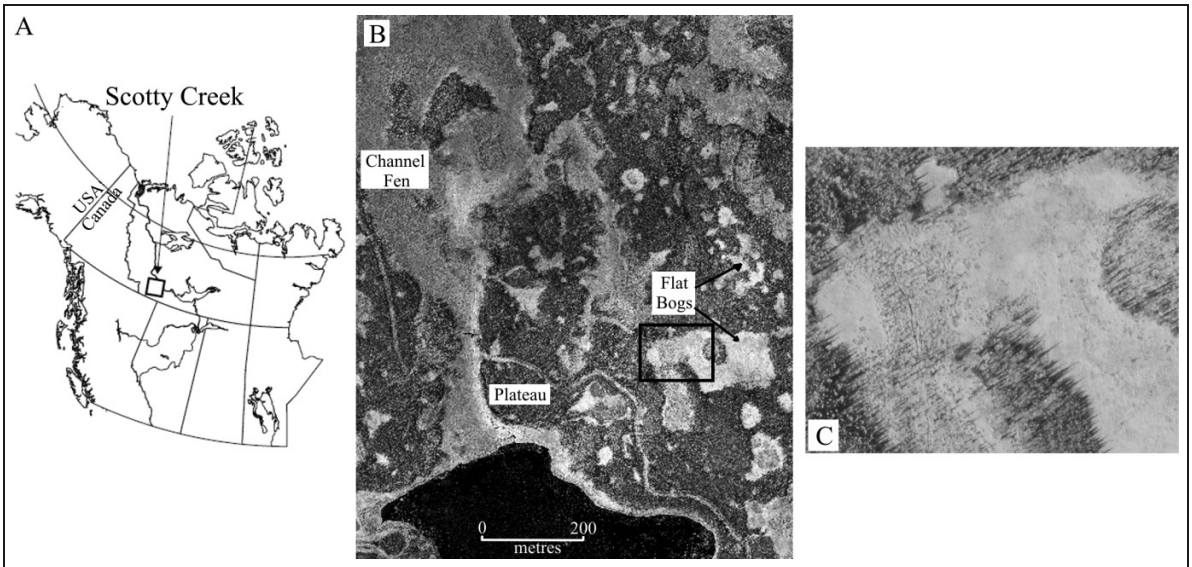

Figure 1. (A) Location of the Scotty Creek study area within the Northwest Territories, Canada. (B) Area examined using aerial photography, IKONOS imagery, and digital imagery. Mosaiced digital imagery (NIR spectral band) illustrates spectral differences between channel fens, plateaus, and flat bogs. (C) Close-up of bog and plateaus represented by black rectangle in (B). Note shadowing from trees (photographs taken at approximately 17:00).

NIR wavelengths. In the VIS wavelengths, plateaus are characterized by relatively low albedo *Picea mariana* (Mill.) canopy (spectrally bright in NIR wavelengths), with a ground covering of shrubs, lichens, and mosses overlying sylvic peat and woody ground material (Quinton et al., 2003). They rise approximately 0.5–2.0 m above the surrounding terrain (Wright et al., 2009; Chasmer et al., 2010), vary in length and width from just a few metres up to approximately 200 m, and often have rounded edges when examined in plan view. Their distinct geometrical and spectral properties are a result of peat development. Peat grows to an elevation that raises the plateau above the water table, thus encouraging establishment of rapidly growing *Sphagnum fuscum* (Schimp.). Growth of *S. fuscum* on plateaus increases mire surface elevation and reduces ground temperature, resulting in the formation of frost bulbs, which further raise the elevation of plateaus (Robinson and Moore, 2000; Quinton et al., 2003). Flat bogs and channel fens are lower in elevation than plateaus and receive drainage water from plateaus. Both also have their own unique spectral (due to overlying vegetation) and geometric properties. Channel fens are characterized by wide (50 m to >100 m), treeless swaths of partially submerged or floating *Sphagnum riparium* (Angstr.) peat. Because peat moss vegetation within fens is often partially submerged or floating and also contains some herbs and shrubs, these surfaces have higher albedo than permafrost plateaus (Quinton et al., 2003) in VIS wavelengths. The exception occurs where standing water (and water-saturated soils) absorbs electromagnetic radiation, thereby reducing albedo (in both VIS and NIR). Flat bogs are often hydrologically connected and are characterized by lower elevations and some woody vegetation located along the plateau–bog margins. Bog vegetation is spectrally the brightest of all land cover types because *Sphagnum* species overlie yellow-coloured peat (Quinton et al., 2003). Thus all main land cover types (plateau, channel fen, and flat bog) are easily distinguishable within VIS and NIR spectral bands found in airborne and spaceborne optical imagery (**Figure 1**) and NIR-intensity lidar data.

Methodology

Lidar data collection and processing

Discrete return airborne lidar data were used at Scotty Creek to map the three-dimensional characteristics of the vegetation canopy and ground surface topography at high resolutions (e.g., Wehr and Lohr, 1999; Lindsay et al., 2004; Hopkinson et al., 2005). Lidar (and digital image) data were collected and processed by the authors at the Applied Geomatics Research Group (Nova Scotia, Canada) on 6 August 2008 using an Airborne Laser Terrain Mapper (ALTM) 3100 (Optech, Inc. Toronto, Ont.) discrete return sensor capable of retrieving one to four returns. The specifications for the lidar survey were defined to ensure adequate ground penetration and full coverage (all sides) of tree canopies. Thus a flying height of 1300 m above ground level (agl), a scan angle of $\pm 18^{\circ}$ with 50% overlap of scan lines, and a pulse repetition frequency of 71 kHz were used. This resulted in up to 10 returns per square metre due to the multiple-return characteristics of the system.

After initial processing, flight line adjustments (strip matching), filtering of outliers, and subsetting, laser returns were classified into ''ground,'' ''vegetation,'' and ''all'' returns in TerraScan software (Terrasolid, Finland). Ground returns (within 0.3 m of the ground surface) were used to create a 1 m $\times$ 1 m digital elevation model (DEM) from which all

aerial photographs were orthorectified. The DEM was created within the software Surfer (Golden Software Inc., Golden, Colo.) using an inverse distance weighting algorithm (O'Sullivan and Unwin, 2003) with an x, y search radius of 2 m and a power of one, such that the return integrity (ground surface morphology determined from a number of points to reduce propagation of error in z height) was maintained.

Image processing and analysis

Historical imagery was acquired on five dates using various RS systems. These included three aerial (VIS panchromatic) photographs dating from 1947, 1970, and 1977; 18 mosaiced (NIR panchromatic) digital images acquired in 2008 (during the lidar survey); and one IKONOS (red–green–blue (RGB), NIR) reflectance image (**Table 1**). Aerial photographs were collected in film format and rescanned at 1600 dpi at the National Air Photo Library, Ottawa, Ont. The 2008 digital images were acquired coincident to and integrated with the ALTM 3100 between 17:00 and 18:00 (local time). All positional information used to locate laser returns was also used to solve exterior orientation parameters of images, camera projection centre coordinates, and attitude parameters. Thus, the coincident lidar and digital image data were geometrically corrected to each other using ground and aerial GPS and inertial measurement unit-assisted triangulation within postprocessing. All historical aerial photographs, digital images, and IKONOS satellite imagery were obtained between mid-June and the beginning of September, rendering images seasonally comparable. This is especially important for change detection analysis in wetland–upland environments where seasonal soil moisture (target wetness) alters albedo at the boundaries between plateaus and bogs–fens. **Table 2** describes the attributes of each of the four cameras used to acquire photographs – digital images.

The combined lidar and digital imagery (2008) was used to aerially triangulate and orthorectify historical aerial photographs. Digital images were mosaiced, clipped, colour-balanced, and orthorectified (using 40–60 tie points per image) within Terraphoto software (Terrasolid, Jyväskylä, Finland) (**Figure 2**). Average tie point adjusted position was reduced from 45.78 to 35.60 cm due to aircraft heading, roll, and pitch. Aerial photographs from 1947 to 1977 (**Figure 2**) were processed differently from the 2008 digital NIR imagery. Photographs were imported into Geomatica software (PCI Geomatics, Ottawa, Ont.), corrected using fiducial marks and camera calibration specifications, and adjusted–rotated using eight carrying geometry over time (multitemporal) tie points. Tie points were located on static man-made objects found in all three aerial photographs within an approximate 3.0 km $\times$ 2.5 km area. Adjusted photographs were then subset into smaller areas based on the region of interest (determined from airborne lidar) and existence of linear features. Photographs were linearly enhanced to emphasize spectral differences between land cover types and subjected to additional aerial triangulation and orthorectification in Ortho Engine (PCI Geomatics) using the 1 m $\times$ 1 m 2008 lidar DEM and digital imagery. Aerial triangulation and orthorectification were performed based on the selection of additional (one time point) tie points per image set (1947 and 2008; 1970 and 2008; and 1977 and 2008). Analysis of aerial photography in stereo perspective using diapositives was not performed because the elevational change of plateaus was often less than the

Table 1. Photograph and image acquisition specifications.

Date and approx. local time of acquisition	Image No.	Type	Altitude	Resolution (m)	Approx. solar elevation (°)	Brief methods
24 July 1947, 13:30	A11019-248	VIS panchromatic aerial photograph	6097 m	0.76	47[a]	Multitemporal aerial triangulation, aerial triangulation, and orthorectification using 2008 aerial photography and lidar
29 August 1970, 14:00	A21530-239	VIS panchromatic aerial photograph	8744 m	1.10	38	Same as per 1947 photograph
12 June 1977, 11:00	A24770-163	VIS panchromatic aerial photograph	4696 m	0.53	40	Same as per 1947 photograph
4 September 2000, 10:30	PO 50558	RGB, NIR IKONOS satellite imagery	681 km	4.00	23	Atmospherically and geometrically corrected
6 August 2008, 18:00	na	NIR digital aerial photography	1300 m	0.18	29	Located using position orientation system (POS) coincident with lidar survey; 18 images stitched with vignettes removed

Note: na, not available.
[a]Shadows in the 1947 image are difficult to discern due to degradation of film image. This is an estimate.

Table 2. Attributes of cameras used to acquire photographs and digital images.

Date of image acquisition	Camera	Lens	Film	Focal length (mm)
24 July 1947	OSC 112	195618	Super XX	152.400
29 August 1970	RC 5A	15 AG 25	2405	152.307
12 June 1977	RC 8	UAG 1020	2405	151.695
6 August 2008	Rollei AIC	Super Angulon AF+ 2.8/50 mm metric	Digital (39 megapixels)	na

Note: na, not available.

resolution of the historical photographs. A smaller area of interest was subset from the IKONOS imagery to match the area of interest of the historical imagery. The IKONOS subset was then geographically compared with the lidar–digital imagery of the same area. No shift in the data (2000 versus 2008) was observed or measured (due to IKONOS resolution). The NIR channel was used for comparison with the 2008 (NIR) mosaiced images (**Figure 2**), such that all images were gray scale and spectral differences due to vegetation type and water content between land covers (plateau, bog, and fen) could be observed and classified.

Cumulative error analysis and classification

Cumulative errors were determined using three criteria: (1) point measurement accuracy based on tie points used in aerial triangulation during the orthorectification procedure (e.g., root mean square (RMS) errors and adjustments used

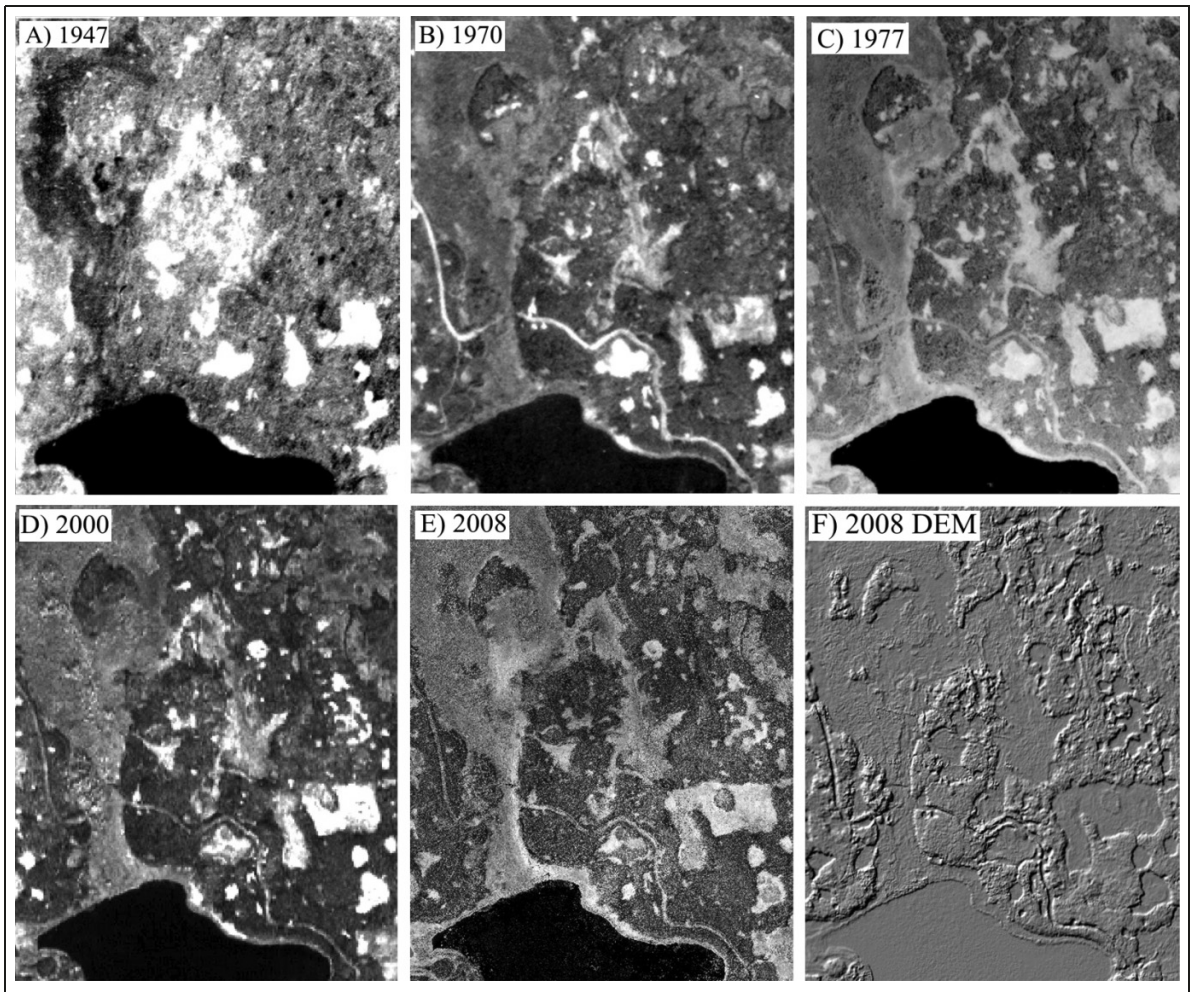

Figure 2. Historic aerial photography (A–C), IKONOS satellite imagery (D), mosaiced digital images from 2008 (E), and a lidar-derived shaded-relief DEM (F).

for image to image and DEM registration), (2) plateau feature detection year after year as a result of variable image radiometric characteristics, and (3) plateau edge delineation and pixel classification accuracy due to variable (image) reflectance of VIS and NIR wavelengths as a result of target soil moisture and canopy shadowing at plateau edges. The procedures used to identify possible errors in total plateau area (per image) are discussed as follows.

(1) Point measurement accuracy following image block rotation and adjustment was determined from tie points used to triangulate historical aerial photography to the 2008 orthophoto–lidar DEM. A total of nine tie points were used to orthorectify the 1947 photograph, 10 to orthorectify the 1970 photograph, and 12 to orthorectify the 1977 photograph. RMS error from individual tie point errors (in x and y) was used to identify possible feature misalignments (registration errors) within historical aerial photographs when compared with the 2008 dataset.

(2) Following the aerial triangulation–orthorectification procedure, plateaus were delineated to separate them from bogs and fens. The process of plateau delineation may also introduce errors in total plateau area extent within the photograph–images. Unfortunately, direct quantification of edge delineation (e.g., using in situ measurement of depth to permafrost and GPS) was impossible for images dating pre-2008. Despite these difficulties, attempts were made to quantify plateau delineation errors using a variety of techniques. Photograph–image tree coverage (representing plateau area) was manually delineated using a combination of (*i*) image thresholding (division of spectrally bright (high albedo) – intermediate (bogs and fens) and dark (low albedo) (treed plateaus) areas); (*ii*) tree canopy shadow modelling (to reduce overestimating plateau area as tree shadows extend into fens–bogs); and (*iii*) visible remnant plateau edges from previous years. A number of classification procedures were also applied, with up to 40 training areas selected per land cover type. However, all classifications suffered from an inability to classify water-saturated (low albedo) and dry (high albedo) areas within bogs and fens. The confusion between land cover types per image was large (>30%), and therefore it was decided that permafrost plateau edges should be manually delineated using the criteria mentioned previously. The manual delineation resulted in two land cover types: (*i*) permafrost plateaus, and (*ii*) bogs and fens. Bogs and fens were not separated from each other because plateau change will always result in conversion to fen or bog. Accuracy of manual delineation was qualitatively examined using two methods. The first method compared four features with varying and similar spectral characteristics to determine if these could be delineated each year. The second method used comparisons between digital image plateau delineation (based on spectral changes in vegetation canopy in 2008) and changes in ground elevation from lidar (used to delineate plateau area as a rise in elevation from surrounding bogs–fens).

(3) Accuracy of edge delineation was determined for 2008 imagery–DEM using GPS validation from in situ transect measurements of the depth to the active layer. Hand-held GPS measurements (WAAS enabled Garmin 250, accuracy of ± 2 m to ± 10 m) were used to locate the boundary between plateau and fen–bog, determined by pushing a metal measurement rod into the soil until permafrost was encountered (e.g., Chasmer et al., 2010). GPS and depth to permafrost measurements were determined for 14 locations during the summer for 2007–2009. GPS locations of plateau edges were then compared with those of delineated (DEM and digital image) plateaus.

Lastly, errors associated with tree shadowing at plateau edges were examined using a shadow model based on solar zenith and elevation angles at the estimated time of photograph–image acquisition. Assuming vegetation heights did not change between photographs–images, and plateau elevation (and shape) was retained from 1947 to 2008, a digital surface model (DSM) of elevation + canopy height was used to estimate the length of shadows and orientation (on one side of plateaus) per image. The DSM was modelled using an inverse distance weighting (IDW) rasterization procedure at 1 m resolution from "all" 2008 lidar returns based on the maximum return height within a 1 m $\times$ 1 m $\times$ z (height) column throughout the study area. Shadow lengths were then cumulated as maximum (total site plateau area including shadow) and minimum (total site plateau area not including shadow) errors.

Cumulative errors due to plateau area overestimation or underestimation (m^2 and percent difference) as a result of delineation errors were estimated. Based on this error assessment, the temporal interval required to observe discernable change in plateau area between two historical images (this site only) was estimated, bearing in mind that cumulative error is exaggerated relative to typical errors and is a "worst-case scenario."

Results and discussion

Point measurement accuracy based on tie point analysis

Aerial photographs taken in 1970 and 1977 show clear-cut lines and paths that were used as a basis for aerial triangulation, thereby reducing the root mean square error (RMSE) significantly from that of the initial (large area) photograph adjustment. In 1970 and 1977, 10 and 12 tie points, respectively, were selected within the 900 m $\times$ 1150 m subarea, most of which registered path intersections between the historical image and the 2008 DEM–mosaiced imagery. Accounting for differences in resolution, tie point RMSEs were $x = 1.03$ m and $y = 0.93$ m for 1970 and $x = 0.92$ m and $y = 0.56$ m for 1977, with average pixel shifts of $x = 0.77$ m and $y = 0.70$ m (<1 pixel (~84% of pixels)) for 1970 and $x =$

0.73 m and y = 0.46 m (~1.38 pixels) for 1977 when orthorectified to the 2008 data. The largest deviations in tie points occurred when locating points on natural features (e.g., sides of ponds, tie points 1, 2 (1970), and 5 (1977)) (**Figures 3B** and **3C**). In 1947, nine tie points were found and located on natural features (**Figure 3A**). Placement of tie points on natural features resulted in larger errors (i.e., larger than those in 1970 and 1977) because discernable, unchanging features could not be found (e.g., Korpela, 2006). The tie point RMSE in 1947 was x = 1.13 m and y = 1.2 m, with a pixel shift of x = 0.88 m and y = 0.88 m (1.15 pixels). In all images, locating tie points to the north of the study area (beyond those used in the initial adjustment) was difficult because unchanging features could not be found. Thus orthorectification errors increased in areas where there were few local tie points. This illustrates why direct comparisons between images (e.g., image subtraction) should be used with caution, as was also noted in Chen et al. (2003). **Figure 3** shows the location and shifts in tie points between the historical imagery and the 2008 DEM–imagery.

Feature detection

Visual comparisons and possible errors were examined by identifying complex (easily confused) areas (area 1) and easily discernable areas (areas 2, 3, and 4), as shown in **Figure 4**. The 1947 aerial photograph was the most difficult to delineate within area 1 and was likely most prone to feature identification and edge delineation errors. Area 1 contains complex saturated depressions that absorb radiation and appear darker in all historical images. Confusion between land covers in the 1947 image is complex (due to image quality, poor lenses used, and nitrate film). Clear boundaries that may or may not be plateau cannot be identified beyond the classification shown in **Figure 4**. During the years 1970, 1977, 2000, and 2008 (**Figures 4B**, **4D**, and **4E**), identification of plateau edges is easier, except for possible mixed pixels at land cover boundaries. In 1970, plateau area was only very slightly smaller than the plateau area in 1977 (1% difference), corresponding to minimal changes in annual average air temperature (four cool years and three warm years; standard deviation = 1.12 °C) measured at Fort Simpson (located within 20 km of the study area). This confirms similarity of identification and classification of plateaus in 1970 and 1977.

Feature detection of the permafrost plateau in area 2 is relatively uncomplicated during all years except 1947 (**Figure 4A**). In 1947, the feature is barely discernable and has been delineated as a large area containing similar spectral properties. Similar spectral properties may be due to

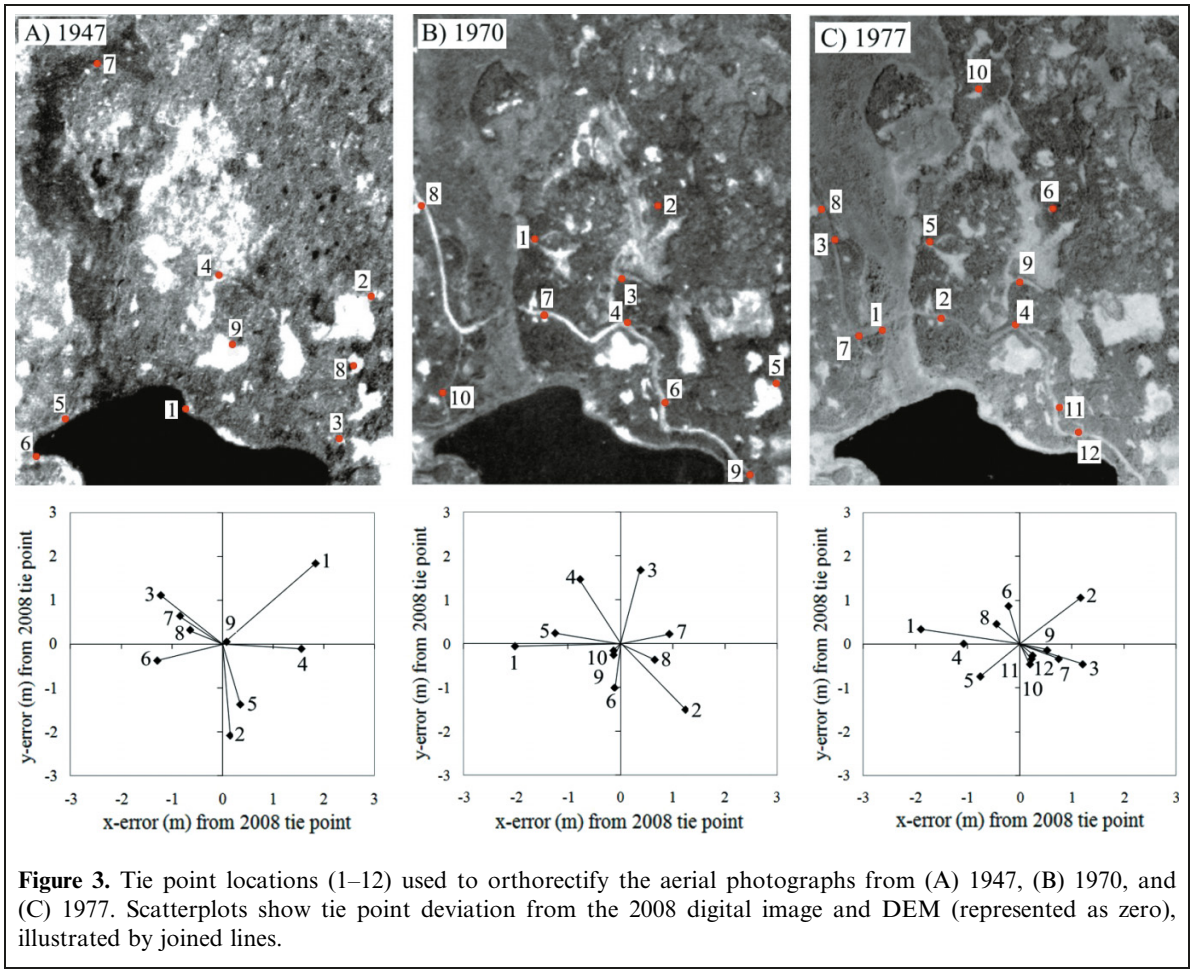

Figure 3. Tie point locations (1–12) used to orthorectify the aerial photographs from (A) 1947, (B) 1970, and (C) 1977. Scatterplots show tie point deviation from the 2008 digital image and DEM (represented as zero), illustrated by joined lines.

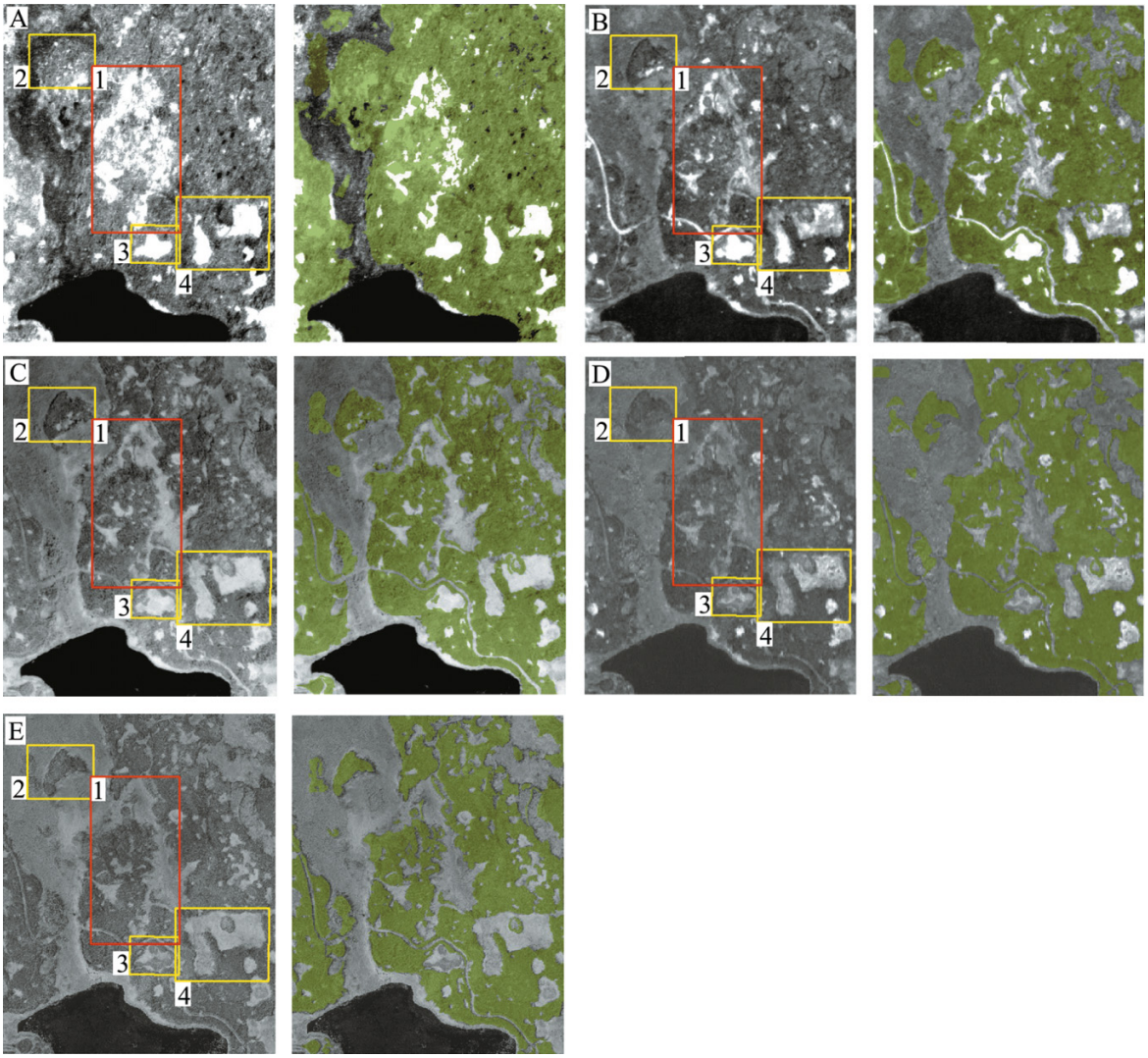

Figure 4. Historical aerial photography, satellite imagery, and digital imagery and manually delineated permafrost plateaus (image to the right of main imagery showing green delineated plateaus): (A) 1947; (B) 1970; (C) 1977; (D) 2000; (E) 2008. Red rectangle (1) outlines an area where permafrost plateaus have been difficult to identify due to differences in soil moisture. The yellow rectangles (2, 3, and 4) in each image outline easily identifiable bogs and plateau edges.

camera sensitivity (e.g., wavelengths used) and image degradation or may be a result of seasonal conditions (e.g., soil moisture). Unfortunately, without validation at the time of acquisition, it is impossible to quantify absolute errors associated with area 2 plateau delineation in 1947.

Despite an inability to directly quantify plateau area using in situ measurements, rates of change per year between acquisition dates may be used as a proxy indicator of plateau detection accuracy, unless image-related errors have the same effect in all areas. This hypothesis ignores differing rates of thaw found in highly fragmented plateaus as opposed to large, nonfragmented plateaus (e.g., Chasmer et al., 2010). **Table 3** shows rates of change per year between acquisition dates, and **Table 4** illustrates percentage differences between rates of change per year for each of the three areas. Small percentage differences in rates of change between areas may indicate more accurate feature delineation, whereas large percentage differences may be indicative of possible errors in feature delineation.

Low percent differences in rates of change between areas 2 and 3 and between areas 3 and 4 for three of four comparison periods (between acquisition dates) (**Table 4**) indicate that plateaus follow similar rates of change between the two areas and may be fairly accurately delineated. Differences in rates of change between areas 2 and 4 are large for all years except 1947–1970, indicating that area 4 may be prone to errors in plateau delineation. Area 4 has a series of saturated zones that cause confusion between land cover types and plateau delineation. The most accurate delineations, assuming that plateaus in the three areas thawed at similar rates, were

Table 3. Annual percent change in area from plateau to bog–fen determined from manual delineation of permafrost plateaus in areas 2, 3, and 4.

Years of comparison[a]	Area 2	Area 3	Area 4
1947–1970 (23)	1.17	0.74	0.81
1970–1977 (7)	0.38	−0.28	0.17
1977–2000 (23)	0.44	0.06	0.11
2000–2008 (8)	1.83	1.35	0.74

[a]Number of years between acquisition dates is given in parentheses.

between 1970 and 1977 imagery (**Table 4**), whereas largest differences in rates of thaw were between 1970 and 2000 imagery and between 2000 and 2008 imagery (likely due to IKONOS pixel resolution).

Combining digital images, lidar data, and in situ GPS measurements of plateau edges and location is the only method for which the accuracy of plateau delineation can be directly quantified (using 2008 data only). Area coverage of plateaus determined using digital imagery (based on vegetation cover) overestimated plateau area by 8% when compared with that of plateaus delineated using the 1 m resolution lidar DEM. Correspondence between DEM-derived plateaus versus vegetation-classified plateaus was 93% and 86%, respectively. This indicates that 7% (14%) of plateaus determined using the lidar DEM (digital images) did not correspond to vegetation cover from digital images (raised uplands from DEM). Differences between DEM and vegetation coverage of plateau areas were often due to woody vegetation extending beyond plateau edges, into bogs and fens. It is likely that this occurs in historical photographs as well, but the extent to which this occurs (and the associated error) remains unknown.

Plateau edge delineation

Permafrost plateaus shed water along their outer margins, resulting in water-saturated soils at plateau–bog–fen edges (e.g., Wright et al., 2009). This results in confusion and possible misclassification between low-albedo trees and saturated ground. Geographically located transect measurements of frost table depth through plateaus and bogs–fens (e.g., Chasmer et al., 2010) indicate that the width of the transition area between plateaus and bogs–fens is within 1–2 m, which is greater than the pixel resolution of all but the IKONOS imagery. Comparisons between plateau edges (determined using hand-held GPS, digital image, and DEM) show that 10 of 14 GPS locations were within 1 m of the lidar DEM delineated permafrost plateau–bog–fen boundary, two were within 6 m of the DEM boundaries, and two were vastly different (by 21 and 34 m, respectively; possibly due to transcription errors). Comparisons between edges based on vegetation cover from digital imagery (2008) and GPS measurement locations show slightly larger errors. These result from tree structures (either alive or dead) extending into bogs–fens. Ten of 14 GPS locations were within 3 m of plateau edges, whereas the remaining edge locations were between 7.3 and 35 m from plateau edges (two of which were possibly due to transcription errors). It is likely that hand-held GPS location errors also contributed to part of this mismatch in edge delineation–validation.

Table 4. Percent differences in rates of change between areas (if two or three areas have minimal percent differences, then they may be changing at close to the same rate per year).

Years of comparison[a]	Areas 2 and 3	Areas 3 and 4	Areas 2 and 4
1947–1970 (23)	36	7	31
1970–1977 (7)	28	38	56
1977–2000 (23)	84	35	75
2000–2008 (8)	26	45	60

[a]Number of years between acquisition dates is given in parentheses.

Shadowing by the canopy at plateau edges, determined from solar azimuth angle and elevation at the approximate time of survey, resulted in variable shadow lengths per photograph–image (**Table 5**).

Using a natural breaks (Jenks) method to classify minimum, average, and maximum ranges in the frequency of canopy heights, 13% of trees were shorter than 1.97 m, 72% of trees ranged in height between 1.97 and 5.00 m, and 15% of trees exceeded 5.00 m in height (**Figure 5**). Based on the average range of canopy heights (1.97–5.00 m) found at the edge of plateaus, solar azimuth angles (**Table 5**), shadow lengths, and pixel resolution, total site plateau area could be overestimated by up to 6% (2008), 10% (2000), 3% (1977), 3% (1970), and 2.8% (1947). Errors in plateau area due to shadowing are also influenced by increased fragmentation within the landscape (e.g., as a result of pixel resolution and the increased development of isolated bogs and stream channels with plateau thaw). Plateau edges (as a percentage of the total area of plateaus, i.e., plateau perimeter to area ratio) increased from 2.5% in 1947 to 3.6% in 1970, 3.8% in 1977, 4.6% in 2000, and 11.8% in 2008, indicating increased fragmentation (more perimeter, less area) of plateaus during recent years.

Table 5. Maximum, minimum, and mean canopy shadow lengths per photograph–image modelled using maximum canopy height and elevation (DSM) determined from lidar (assuming vegetation height and plateau elevation did not vary from 1947 to 2008).

Date of acquisition	Solar azimuth angle (°)	Shadow length (m)		
		Max.[a]	Min.[b]	Mean[c]
24 July 1947	165.4	7.6	1.0	4.1
29 August 1970	178.1	5.9	0	3.8
12 June 1977	119.0	4.4	0	2.8
4 September 2000	61.2	13.7	0.3	7.8
6 August 2008	248.0	10.1	0.4	5.4

[a]Maximum canopy height = 10.3 m.
[b]Minimum canopy height = 0.26 m.
[c]Mean canopy height = 3.49 m.

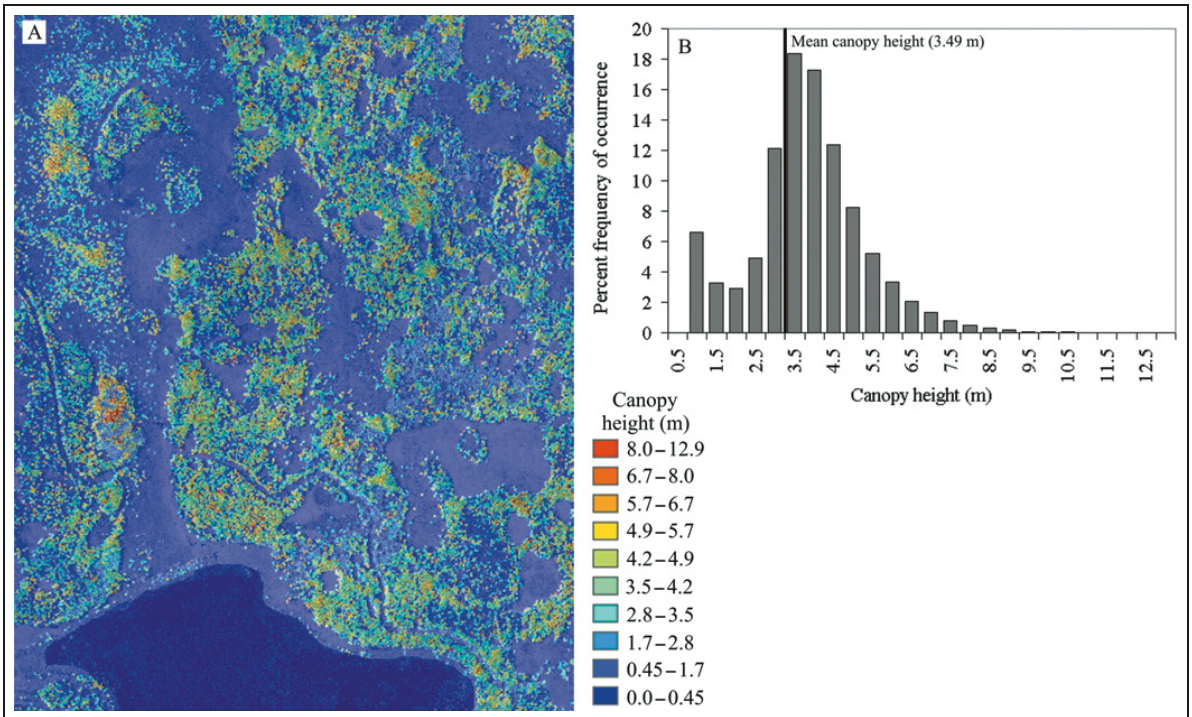

Figure 5. (A) Lidar-derived canopy height model (CHM) overlain on the 2008 aerial photographs. (B) Percent frequency of occurrence of canopy heights found within the study area.

Cumulative error and temporal interval required to observe discernable changes in plateau area

Figure 6 shows maximum and minimum (worst case) cumulative error due to aerial triangulation – orthorectification, pixel resolution, delineation errors, and shadowing. Strictly speaking, cumulative errors as a percentage of permafrost area (**Figure 6A**) are not entirely correct because permafrost area is changing. Cumulative error of the site (**Figure 6B**) is a more appropriate measure of error per image and pixel resolution. Images acquired in 1977 and 2008 have the lowest errors (8% and 10%, respectively), and 2000 IKONOS imagery has the highest error (26%). Permafrost plateau area rates of change, including all photographs–imagery, decreased by 0.5% of the total area approximately every year (determined from linear correlation, $r^2 = 0.91$). Chen et al. (2003) found similar rates of simulated change within the discontinuous permafrost zone from 1940 to the late 1980s when examining results of a hydrological runoff model, remote sensing, soil, and climate inputs. Given maximum–minimum cumulative errors examined in this study, approximately 21 years were required to detect change from digital imagery at a resolution of 0.18 m. As resolution decreased, the number of years required to determine discernable change (beyond errors) increased to 32 years at 1.1 m resolution and 60 years at the resolution of an IKONOS image (4 m). Of course, there are numerous limitations to these generalizations, and these periods are estimates based on the sensitivity analysis provided. The results illustrate the importance of very high resolution imagery for permafrost plateau change assessment in the discontinuous permafrost zone (Chen et al., 2003). Lower resolution imagery (e.g., Zhang et al., 2004) and poor quality (old) photographs are not recommended for detailed analysis of permafrost plateau change at Scotty Creek. These may be more appropriate for large area mapping of permafrost change or areas where permafrost is thawing more rapidly.

Error assessment limitations

The quantification of permafrost plateau area change and error analysis using historical RS datasets has many limitations, especially evident in this study. These include aerial triangulation – orthorectification issues (e.g., use of minimal number of tie points), film quality and degradation, radiometric normalization issues (e.g., vignetting, atmospheric influences, and bidirectional reflectance distribution function), lack of in situ plateau edge measurements using GPS pre-2008, soil target wetness, and lidar ground return accuracy in dense vegetation. These issues are discussed in the following.

In this study, point measurement accuracy was determined on the basis of the user's ability to select multitemporal tie points (historical aerial photograph adjustments), and one time point tie points between historical photographs and data from 2008. Selected features often consist of roads with intersections, parking lots, buildings, etc. In the case of remote areas within the Canadian subarctic, such as the Scotty Creek study area, finding locations appropriate for tie points can be difficult because the environment is rapidly

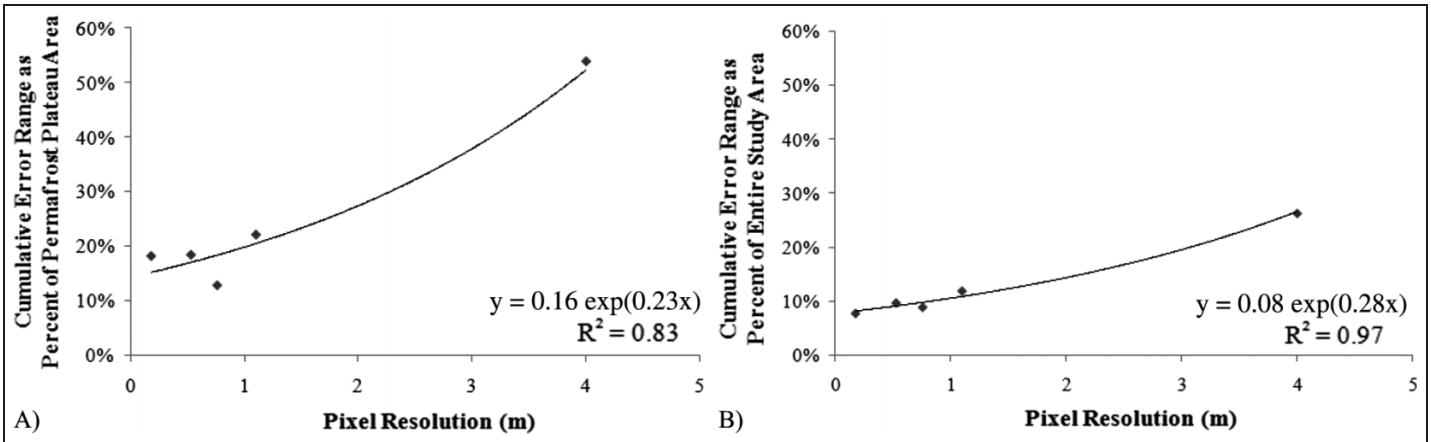

Figure 6. Percent cumulative error (maximum and minimum) per pixel resolution based on the total area of permafrost plateaus (A) and the entire study site area (B).

changing and the extent of human development is typically limited. Further, application of calibration versus validation tie points to reduce uncertainty in these areas is almost impossible because of a lack of stable features. An inability to properly locate tie points between images leads to errors in point measurement position.

Poor film quality and degradation, especially evident in the 1947 aerial photograph, can result in blurred images and difficulties with radiometric normalization. Korpela (2006) noted that errors due to film deformation may result from poor storage practices and severe lens distortion. Distortion errors may be reduced or eliminated during the fiducial mark transformations (applied to all photographs used in this study) (Korpela, 2006), however, issues with radiometric normalization, especially pre-1960, cannot be corrected. Differences in image brightness (e.g., due to vignetting, sun glint, and atmospheric influences) cause confusion when delineating or classifying permafrost plateaus. It may be the case that some images dating pre-1970 may be too poor for accurate permafrost plateau delineation using forest cover.

A lack of in situ measurements of permafrost plateau edges using survey-grade GPS (or less accurate hand-held GPS) at Scotty Creek may be one of the biggest limitations. Comparisons of plateau area using historical and current aerial photography, digital imagery, and airborne lidar require accurate validation of plateau edges (in combination with rod measurements of the depth to permafrost). Unfortunately, it is impossible to provide validation for past RS data collections, and thus it is essential that validation of current and future campaigns is performed. Strictly speaking, differentially corrected, survey-grade GPS (with rover and base station) should always be used when evaluating land cover types using high-resolution (e.g., $<$4 m) RS data (e.g., Hopkinson et al., 2005; Morsdorf et al., 2006). Survey-grade GPS often has better than 1 m positional accuracy, which is suitable for the 1–2 m transition zone between plateau edges and bogs–fens, and high-resolution imagery. More often than not, easily accessible hand-held GPS units are used to obtain positional information, which is then compared with high-resolution RS data products. Unfortunately, the accuracy of hand-held units ranges from $\pm$2 m to $\pm$10 m, which is often greater than the pixel resolution. In this study, exaggeration of DEM versus digital image plateau edge errors determined from in situ measurements may have resulted from the use of hand-held GPS units.

Soil (target) saturation–wetness has not been quantitatively assessed in this study but likely contributes to over-exaggeration of plateau area due to spectral confusion with tree canopies. Surface depressions and areas of water accumulation may be determined using airborne lidar DEMs and (or) reduced laser return intensity (e.g., Garroway et al., 2010), however, it is not guaranteed that depressions will yield high surface soil moisture content at the time of historical RS data collection. Future studies that use airborne lidar to delineate plateau area should also consider using laser return intensity and absorption at 1064 nm as an indicator of plateau edge (along with elevation information).

Laser return elevational accuracy (and DEM generation) is worse than industry specified–calibrated vertical error in areas of short, dense vegetation. Vertical errors occur when the probability of multiple returns reaching the ground surface is reduced, resulting in returns lying above the ground surface, within vegetation (Töyra et al., 2003; Hopkinson et al., 2005; Bowen and Waltermire, 2007). Returns may also be misclassified as ground (e.g., within Terrascan) when in reality they have reflected from vegetation (e.g., Raber et al., 2002). Hopkinson et al. (2005) found that vertical errors varied as a result of vegetation type, with the largest errors in vertical ground heights occurring within areas of aquatic vegetation (+0.15 m, raw lidar returns; and +0.12 m, rasterized returns). Transition areas between plateaus and bogs–fens are characterized by short, dense grass vegetation and sparse forest cover. Vertical errors in return heights from the ground surface – short vegetation could overestimate plateau area using a lidar DEM in some places if there are few to no returns from the ground surface. However, because

return density is high at this site (e.g., up to 10 returns per square metre), it is likely that some returns will have penetrated to the ground surface within the 1 m resolution of the DEM. Confirmation of this hypothesis may be quantified using differentially corrected, survey-grade GPS (e.g., Hopkinson et al., 2005).

Conclusions

The accuracy of delineating permafrost area using historical aerial photography, digital imagery, satellite imagery, and a lidar DEM was examined in this study using a variety of methods. It is concluded that plateau area delineation is exceedingly difficult using historical imagery that has degraded over time, and potential errors in edge delineation may be impossible to quantify completely and accurately. Despite these issues, a number of methods have been employed to explore a range of possible errors in plateau delineation. Suggestions are also made to improve future RS-based validation campaigns focused on studying permafrost change. The following has been learned.

(1) In some cases, historical aerial photography may be sufficiently degraded to the point where it is very difficult to accurately detect change in permafrost plateau area within the image (using vegetation cover as a proxy). If this is the case, some features may be identifiable, but it may also be impossible to quantify radiometric (and spatial) degradation.

(2) To properly validate current and future RS datasets used to assess plateau change, a statistically significant sample of plateau edges (determined by pushing a measurement rod into the soil to a depth where permafrost exists) must be located using a differentially corrected survey-grade GPS (base station and rover). Hand-held GPS units are not likely accurate enough for in situ permafrost plateau edge detection and high-resolution ($<$2 m) RS analysis.

(3) Where survey-grade GPS measurements of plateau edges do not exist, a lidar DEM may be used to estimate plateau edges based on residual elevation differences from surrounding bogs–fens. This does not provide a true measure of permafrost area, but is likely better than using vegetation cover alone. DEM accuracy, however, depends on a high density of returns per square metre, such that some pulses will penetrate through vegetation to the ground.

(4) In this study, comparisons made between 1977 and 2008 likely provide the best estimate of permafrost area change. This is due to high photograph–image resolution, comparable temporal periods, minimal damage evident in the 1977 image, and the ability to locate and measure canopy shadows at plateau edges. If this is the case, plateau area decreases by approximately 0.5% of the total study area each year. Based on cumulative errors found in this study, 21–32 years are roughly required to observe changes in plateau area at the Scotty Creek watershed (based on $<$1 m resolution). If rates of permafrost degradation increase (decrease) from this estimate, the time interval required between images will decrease (increase).

(5) The resolution of IKONOS imagery (4 m) is insufficient for accurately detecting permafrost edges and change within the current timeline of historical RS data at Scotty Creek ($\sim$60 years). However, it may be more suitable for sites where permafrost is subjected to faster rates of degradation.

Acknowledgements

We are grateful for the lidar data collected and processed by the Applied Geomatics Research Group, Nova Scotia, and assistance from Suzanne Monette (processing of aerial photographs from 2008) and Allyson Fox (processing of lidar data). Peter Whittington and Masaki Hayashi are acknowledged for contributing GPS measurements of plateau–bog–fen edges. Thank you also to the National Air Photo Library, Ottawa, Ont., for maintaining historical photography. We would also like to acknowledge the assistance and detailed comments provided by three anonymous reviewers. This research was funded by the Canadian Foundation for Climate and Atmospheric Sciences (IP3 Research Network), the Natural Sciences and Engineering Research Council of Canada, the Environment Canada Science Horizons Program, and the Northern Scientific Training Program.

References

Beilman, D.W., and Robinson, S.D. 2003. Peatland permafrost thaw and landform type along a climatic gradient. In *Proceedings of the 8th International Conference on Permafrost*, 21–25 July 2003, Zurich, Switzerland. Edited by M. Phillips, S.M. Springman, and L.U. Arenson. A.A. BalkemaLisse, The Netherlands. pp. 61–65.

Boike, J., and Yoshikawa, K. 2003. Mapping of periglacial geomorphology using kite/balloon aerial photography. *Permafrost and Periglacial Processes*, Vol. 14, pp. 81–85.

Bowen, Z., and Waltermire, R. 2007. Evaluation of light detection and ranging (LIDAR) for measuring river corridor topography. *Journal of the American Water Resources Association*, Vol. 38, No. 1, pp. 33–41.

Chasmer, L., Whittington, P., Hopkinson, C., Petrone, R., and Quinton, W. 2010. The influence of vegetation canopy structure on the spatial pattern of active layer thaw within the sub-arctic–boreal transition discontinuous zone. *Permafrost and Periglacial Processes*. In press.

Chen, W., Zhang, Y., Cihlar, J., Smith, S.L., and Riseborough, D. 2003. Changes in soil temperature and active layer thickness during the twentieth century in a region in western Canada. *Journal of Geophysical Research*, Vol. 108, No. D22, p. 4696. doi:10.1029/2002JD003355.

Garroway, K.S., Hopkinson, C., and Jamieson, R. 2010. Investigating the influence of surface soil moisture and vegetation cover on airborne lidar intensity data. *Canadian Journal of Remote Sensing*. In press.

Hayashi, M., Quinton, W., Pietroniro, A., and Gibson, J. 2004. Hydrologic functions of wetlands in a discontinuous permafrost basin indicated by isotopic and chemical signatures. *Journal of Hydrology*, Vol. 296, pp. 81–97.

Hayashi, M., Goeller, N., Quinton, W.L., and Wright, N. 2007. A simple heat-conduction method for simulating frost table depth in hydrological models. *Hydrological Processes*, Vol. 21, pp. 2610–2622.

Hinzman, L.D., Bettez, N.D., Bolton, W.R., Chapin, F.S., and 31 others. 2005. Evidence and implications of recent climate change in northern Alaska and other Arctic regions. *Climatic Change*, Vol. 72, pp. 251–298.

Hopkinson, C., Chasmer, L.E., Sass, G., Creed, I.F., Sitar, M., Kalbfleisch, W., and Treitz, P. 2005. Vegetation class dependent errors in lidar ground elevation canopy height estimates in a boreal wetland environment. *Canadian Journal of Remote Sensing*, Vol. 31, No. 2, pp. 191–206.

Korpela, I. 2006. Geometrically accurate time series of archived aerial images and airborne lidar data in a forest environment. *Silva Fennica*, Vol. 40, No. 1, pp. 109–126.

Lantuit, H., and Pollard, W.H. 2008. Fifty years of coastal erosion and retrogressive thaw slump activity on Herschel Island, southern Beaufort Sea, Yukon Territory, Canada. *Geomorphology*, Vol. 95, pp. 64–92.

Leverington, D.W., and Duguay, C.R. 1997. A neural network method to determine the presence or absence of permafrost near Mayo, Yukon Territory, Canada. *Permafrost and Periglacial Processes*, Vol. 8, pp. 205–215.

Lindsay, J.B., Creed, I.F., and Beall, F.D. 2004. Drainage basin morphometrics for depressional landscapes. *Water Resources Research*, Vol. 40, No. W09307. doi:10.1029/2004WR003322.

Mars, J.C., and Houseknecht, D.W. 2007. Quantitative remote sensing study indicates doubling of coastal erosion rate in past 50 yr along a segment of the Arctic coast of Alaska. *Geology*, Vol. 35, pp. 583–586.

McMichael, C.E., Hope, A.S., Stow, D.A., and Fleming, J.B. 1997. The relation between active layer depth and spectral vegetation index in arctic tundra landscapes of the North Slope of Alaska. *International Journal of Remote Sensing*, Vol. 18, No. 11, pp. 2371–2382.

Morsdorf, F., Kotz, B., Meier, E., Itten, K., and Allgower, B. 2006. Estimation of LAI and fractional cover from small footprint airborne laser scanning data based on gap fraction. *Remote Sensing of Environment*, Vol. 104, pp. 50–61.

National Wetlands Working Group. 1998. *Wetlands of Canada*. Sustainable Development Branch, Environment Canada, Ottawa, Ont., and Polyscience Publications Inc., Ottawa, Ont. Ecological Land Classification Series, No. 24

O'Sullivan, D., and Unwin, D.J. 2003. *Geographic information analysis*. Wiley, Hoboken, N.J.

Peddle, D.R., and Franklin, S.E. 1992. Multisource evidential classification of surface cover and frozen ground. *International Journal of Remote Sensing*, Vol. 13, No. 17, pp. 3375–3380.

Quinton, W.L. and Hayashi, M. 2007. Recent advances toward physically-based runoff modelling of the wetland-dominated, central Mackenzie River Basin. In *Cold region atmospheric and hydrologic studies, the Mackenzie GEWEX Experience, Vol. 2: Hydrologic processes*. Edited by M-K Woo. Springer-Verlag, Berlin, Germany. pp. 257–279.

Quinton, W., Hayashi, M., and Pietroniro, A. 2003. Connectivity and storage functions of channel fens, and flat bogs in northern basins. *Hydrological Processes*, Vol. 17, pp. 3665–3684.

Quinton, W.L., Shirazi, T., Carey, S.K., and Pomeroy, J.W. 2005. Soil water storage and active-layer development in a sub-alpine tundra hillslope, southern Yukon Territory, Canada. *Permafrost and Periglacial Processes*, Vol. 16, pp. 369–382.

Quinton, W.L., Hayashi, M., and Carey, S.K. 2008. Peat hydraulic conductivity in cold regions and its relation to pore size and geometry. *Hydrological Processes*, Vol. 22, pp. 2829–2837.

Quinton, W., Hayashi, M., and Chasmer, L. 2009. Peatland hydrology of discontinuous permafrost in the Northwest Territories: overview and synthesis. *Canadian Journal of Water Resources*, Vol. 34, No. 4, pp. 311–328.

Raber, G.T., Jensen, J.R., Schill, S.R., and Schuckman, K. 2002. Creation of digital terrain models using an adaptive lidar vegetation point removal process. *Photogrammetric Engineering & Remote Sensing*, Vol. 68, pp. 1307–1315.

Riordan, B., Verbyla, D., and McGuire, A.D. 2006. Shrinking ponds in subarctic Alaska based on 1950–2002 remotely sensed images. *Journal of Geophysical Research*, Vol. 111, No. G04002. doi:10.1029/2005JG000150.

Robinson, S.D., and Moore, T.R. 2000. The influence of permafrost and fire upon carbon accumulation in high boreal peatlands, Northwest Territories, Canada. *Arctic, Antarctic and Alpine Research*, Vol. 32, pp. 155–166.

Rouse, W.R. 2000. Progress in hydrological research in the Mackenzie GEWEX study. *Hydrological Processes*, Vol. 14, pp. 1667–1685.

Töyra, J., Pietroniro, A., Hopkinson, C., and Kalbfleisch, W. 2003. Assessment of airborne scanning laser altimetry (lidar) in a deltaic wetland environment. *Canadian Journal of Remote Sensing*, Vol. 29, No. 6, pp. 718–728.

Tutubalina, O.V., and Rees, W.G. 2001. Vegetation degradation in a permafrost region as seen from space: Noril'sk (1961–1999). *Cold Regions Science and Technology*, Vol. 32, pp. 191–203.

Wehr, A., and Lohr, U. 1999. Airborne laser scanning — an introduction and overview. *ISPRS Journal of Photogrammetry and Remote Sensing*, Vol. 54, No. 2–3, pp. 68–82.

Wright, N., Hayashi, M., and Quinton, W.L. 2009. Spatial and temporal variations in active layer thawing and their implication on runoff generation in peat-covered permafrost terrain. *Water Resources Research*, Vol. 45, No. W05414. doi:10.1029/2008WR006880.

Zhang, T., Barry, R.G., and Armstrong, R.L. 2004. Application of satellite remote sensing techniques to frozen ground studies. *Polar Geography*, Vol. 28, No. 3, pp. 163–196.